ENDOR Studies of the Primary Donor Cation Radical in Mutant Reaction Centers of *Rhodobacter sphaeroides* with Altered Hydrogen-Bond Interactions†

J. Rautter,‡ F. Lendzian,‡ C. Schulz,‡ A. Fetsch,‡ M. Kuhn,‡ X. Lin,§ J. C. Williams,§ J. P. Allen,§ and W. Lubitz*,‡

Max-Volmer-Institut für Biophysikalische und Physikalische Chemie, Technische Universität Berlin, Strasse des 17. Juni 135, D-10623 Berlin, Germany, and Department of Chemistry and Biochemistry and the Center for the Study of Early Events in Photosynthesis, Arizona State University, Tempe, Arizona 85287-1604

Received February 28, 1995; Revised Manuscript Received April 19, 1995⊗

ABSTRACT: The electronic structure of the cation radical of the primary electron donor was investigated in genetically modified reaction centers of *Rhodobacter sphaeroides*. The site-directed mutations were designed to add or remove hydrogen bonds between the conjugated carbonyl groups of the primary donor, a bacteriochlorophyll dimer, and histidine residues of the protein and were introduced at the symmetry-related sites L168 His→Phe, HF(L168), and M197 Phe→His, FH(M197), near the 2-acetyl groups of the dimer and at sites M160 Leu→His, LH(M160), and L131 Leu→His, LH(L131), in the vicinity of the 9-keto carbonyls of the dimer. The single mutants and a complete set of double mutants were studied using EPR, ENDOR, and TRIPLE resonance spectroscopy. The changes in the hydrogen bond situation of the primary donor were accompanied by changes in the dimer oxidation midpoint potential, ranging from 410 to 710 mV in the investigated mutants [Lin, X., Murchison, H. A., Nagarajan, V., Parson, W. W., Williams, J. C., & Allen, J. P. (1994) *Proc. Natl. Acad. Sci. U.S.A. 91*, 10265−10269]. It was found that the addition or removal of a hydrogen bond causes large shifts of the spin density between the two halves of the dimer. Measurements on double mutants showed that the unpaired electron can be gradually shifted from a localization on the L-half of the dimer to a localization on the M-half, depending on the hydrogen bond situation. As a control, the effects of the different hydrogen bonds on $P^{\bullet+}$ in the mutant HL(M202), which contains a $BChl_L$−$BPhe_M$ heterodimer as the primary donor with localized spin on the BChl a_L [Bylina, E. J., & Youvan, D. C. (1988) *Proc. Natl. Acad. Sci. U.S.A. 85*, 7226−7230; Schenck, C. C., Gaul, D., Steffen M., Boxer S. G., McDowell L., Kirmaier C., & Holten D. (1990) in *Reaction Centers of Photosynthetic Bacteria* (Michel-Beyerle M. E., Ed.) pp 229−238, Springer, Berlin] were studied. In this mutant only small local changes of the spin densities (≤10%) in the vicinity of the hydrogen bonds were observed. The effects of the introduced hydrogen bonds on the spin density distribution of the dimer in the mutants are discussed in terms of different orbital energies of the two BChl *a* moieties which are directly influenced by hydrogen bond formation. The observed changes of the spin density distribution for the double mutants are additive with respect to the single mutations. This indicates that no major structural changes occur due to the replacement of the amino acid residues. The asymmetric spin density distributions of $P^{\bullet+}$ were compared with electron transfer rates. A pronounced influence was observed on the $P^{\bullet+}$ reduction rate by cytochrome c_2.

The bacterial reaction center (RC)[1] is an integral membrane pigment−protein complex that facilitates the early electron transfer steps in photosynthesis (Feher et al., 1989; Ermler et al., 1994b). The light-induced electron transfer in the RC, which leads to a charge separation across the membrane, is determined by both the spatial and the electronic structure of the cofactors involved in this process. The spatial structure of the RC was determined for two purple bacterial species, *Rhodopseudomonas (Rps.) viridis* (Deisenhofer et al., 1984) and *Rhodobacter (Rb.) sphaeroides* (Allen et al., 1987; El-Kabbani et al., 1991; Chirino et al., 1994; Ermler et al., 1994a). The RC from *Rb. sphaeroides*, which is studied in this work, consists of three membrane-spanning protein subunits, denoted L, M, and H, that bind the cofactors: four bacteriochlorophyll a (BChl *a*) (the molecular structure is shown in Figure 1), two bacteriopheophytin a (BPhe *a*), two ubiquinone molecules (Q_A and Q_B), one non-heme iron, and one carotenoid. Although these cofactors are arranged in two branches (A and B), which are related by an approximate C_2 symmetry axis, the electron transfer occurs only along the active A branch. Photoexcitation of the primary donor P, a BChl *a* dimer, initiates electron transfer to the intermediate acceptor I, a BPhe *a*. Subsequently, the electron is transferred to the primary acceptor

† This work was supported by DFG (Sfb 312, TP A4), TU Berlin (FIP 6/12), NATO (CRG 910468), Fonds der Chemischen Industrie to W.L., NIH (GM45902) to J.C.W., and NSF (MCB-9404925) to J.P.A. This is publication no. 240 from the center for Early Events in Photosynthesis.

* To whom correspondence should be addressed, at Max-Volmer-Institut, Technische Universität Berlin, Strasse des 17. Juni 135, D-10623 Berlin, Germany. Fax: (#4930) 314 21122.

‡ Technische Universität Berlin.

§ Arizona State University.

⊗ Abstract published in *Advance ACS Abstracts,* June 15, 1995.

[1] Abbreviations: EPR, electron paramagnetic resonance; ENDOR, electron nuclear double resonance; TRIPLE, electron−nuclear−nuclear triple resonance; P, primary electron donor; BChl, bacteriochlorophyll; BPhe, bacteriopheophytin; RC, reaction centers; *Rps., Rhodopseudomonas*; *Rb., Rhodobacter*; I, intermediate acceptor; hfc, hyperfine coupling constant; HOMO, highest occupied molecular orbital; HMO, Hückel molecular orbital; dCTP, 2′-deoxycytidine 5′-triphosphate; Tris, tris-(hydroxymethyl)aminomethane; EDTA, Ethylenediaminetetraacetic acid; LDAO, lauryldimethylamine-*N*-oxide; rf, radio frequency; ET, electron transfer; cyt, cytochrome.

0006-2960/95/0434-8130$09.00/0

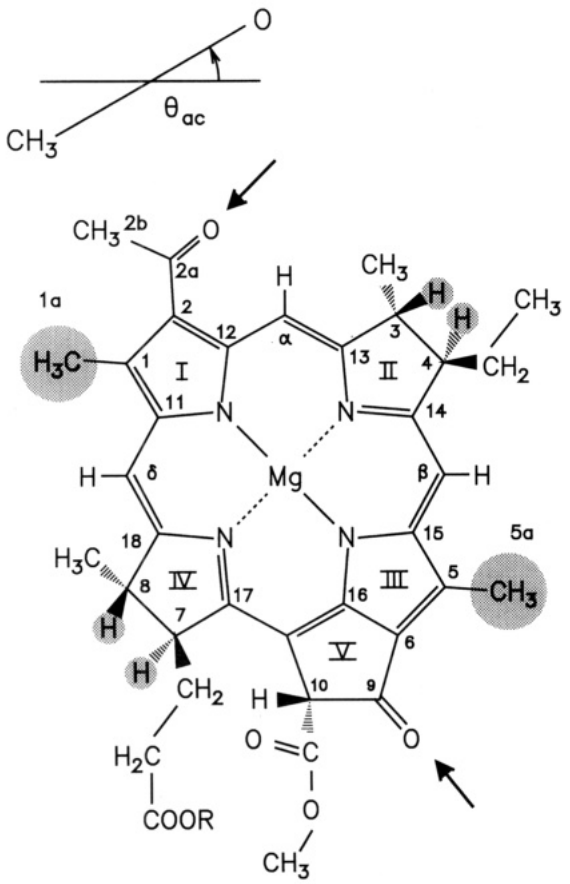

FIGURE 1: Molecular structure of BChl *a*, R = phytyl, including the numbering scheme. The hydrogen positions exhibiting large hfcs in the cation radical are marked by shaded circles. The conjugated carbonyl oxygen atoms that act as hydrogen bond acceptors in the mutants are indicated by arrows. The insert (top) shows the definition of the $C_{12}-C_2-C_{2a}-O$ dihedral angle θ_{ac}. For $0 < \theta_{ac} < 180$ the oxygen atom lies above the plane of the figure.

Q_A and finally to the secondary acceptor Q_B. The primary donor is at the interface between photophysical and chemical processes, i.e., exciton and electron transfer, and is therefore of particular interest. After the electron is transferred, the cation radical of the primary donor $P^{\bullet+}$ remains.

The electronic structure of $P^{\bullet+}$ in its relaxed state is obtained from the electron−nuclear hyperfine couplings (hfcs). After assignment of the measured hfcs to individual molecular positions, a map of the spin density distribution of the unpaired valence electron is obtained for the highest occupied molecular orbital (HOMO) of P. To obtain the hfcs, "hyperfine spectroscopy" techniques, such as electron nuclear double resonance (ENDOR) and electron−nuclear−nuclear triple resonance (TRIPLE), can be employed [see Lubitz (1991), Möbius et al. (1989), and Hoff (1993) for reviews]. Extensive EPR and ENDOR studies of the cation radical $P^{\bullet+}$ in RC single crystals of *Rb. sphaeroides* R-26 revealed an unequal distribution of the π-spin density with a ratio of 2:1 in favor the L-half of the special pair, P_L (L and M subscripts denote the protein subunit to which the cofactors are bound) (Lendzian et al., 1993). The same ratio of 2:1 is also found for $P^{\bullet+}$ in other purple bacteria that possess a BChl *a* dimer as the primary donor (Rautter et al., 1994) and for the Bchl *b* containing bacterium *Rps. viridis* (Lendzian et al., 1988). The observed asymmetry was explained by energetic differences of the HOMOs of the

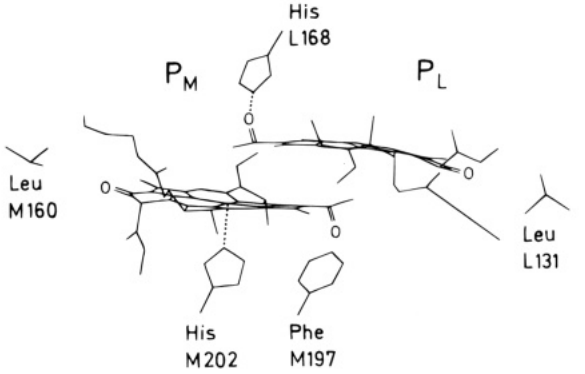

FIGURE 2: Structure of the two Bchls of the primary donor P_L and P_M with the the amino acid residues exchanged by site-directed mutagenesis. Residues Leu M160, Leu L131, and Phe M197 are replaced by histidine, residue His L168 is replaced by phenylalanine, and the His M202 is replaced by a leucine. The hydrogen bond between His L168 and the oxygen of the 2-acetyl group of P_L and the ligation of His M202 to the central Mg^{2+}-ion of P_M in the wild type are indicated by dashed lines. Structure using the coordinates from Ermler et al. (1994a) (Brookhaven PDB entry 1PCR).

monomeric halves P_L and P_M of the special pair on the basis of a simple Hückel molecular orbital (HMO) model dimer (Plato et al., 1992; Lendzian et al., 1993; Rautter et al., 1994). The energetic difference between the two BChl *a* molecules P_L and P_M originates in different protein environments of the two halves, which leads to different conformations of P_L and P_M. The method of choice to investigate the effects of the protein−cofactor interactions, i.e., the impact of specific amino acid residues on the spin density distribution of $P^{\bullet+}$, is site-directed mutagenesis.

One of the most direct ways that a protein can interact with a bacteriochlorophyll is through hydrogen bonds to the carbonyl groups. In BChl, the 2-acetyl and 9-keto groups are part of the conjugated π-system (Figure 1), and bonding to these groups should have a direct effect on the electronic structure. Figure 2 shows the structure of the BChl *a* dimer together with five amino acid residues: M160, M197, M202, L131, and L168 as obtained from the X-ray structure (Ermler et al., 1994a). In wild-type RCs of *Rb. sphaeroides* only one hydrogen bond is formed between the 2-acetyl group of P_L and the residue His L168 (see Figure 2). Thus, the hydrogen bonding arrangement is asymmetric in the wild type. To investigate the influence of hydrogen bonding interactions on the properties of the donor, a series of mutants was designed to introduce or remove hydrogen bonds to the special pair (Williams et al., 1992b; Murchison et al., 1993; Lin et al., 1994a). The individual mutations in the vicinity of the 2-acetyl groups of the dimer are His to Phe at position L168 [mutant HF(L168)], designed to remove the hydrogen bond to the 2-acetyl group of P_L and Phe to His at position M197 [mutant FH(M197)], with the aim to add a hydrogen bond to the 2-acetyl group of P_M. The mutations Leu to His at position M160 [mutant LH(M160)], and Leu to His at position L131 [mutant LH(L131)] were designed to add a hydrogen bond to the 9-keto carbonyls of P_L and P_M. A complete set of *all* the double mutant combinations of these amino acid residues has been constructed. These include a mutant with two new hydrogen bonds in symmetrical positions [mutant LH(M160) + LH(L131)] and another mutant with a hydrogen bond to P_M rather than P_L [mutant HF(L168) + FH(M197)]. The formation or removal of the respective hydrogen bonds has been confirmed by results

from fourier transform infrared (FTIR) (Nabedryk et al., 1993) and resonance Raman spectroscopy (Mattioli et al., 1994, 1995).

The addition or removal of these hydrogen bonds leads to a significant increase or decrease of the oxidation midpoint potential of P in these mutants. It has been shown for the double mutants that a combination of the mutations produces changes in this potential, which are additive with respect to the single mutants (Lin et al., 1994a). The oxidation midpoint potentials of P in the mutants cover a range of 410−710 mV in comparison to 505 mV for *Rb. sphaeroides* wild type. In this paper we present an EPR and ENDOR characterization of the effects of these mutations on the spin density distribution of $P^{\bullet+}$. Preliminary results obtained from part of these mutants (Rautter et al., 1992) showed pronounced effects on the spin density distribution of $P^{\bullet+}$. A mutant with the addition of a hydrogen bond to the 2-acetyl group has also been reported for the RC of *Rhodobacter capsulatus* (Stocker et al., 1992); this mutant also showed an increase in the donor midpoint potential as FH(M197) in *Rb. sphaeroides*.

High oxidation midpoint potentials of P can also be expected for the combination of the hydrogen bond mutations with one of the heterodimer mutants of *Rb. sphaeroides*, HL-(M202). The exchange of the histidine residue in position M202, which acts as an axial ligand to the central Mg^{2+} ion of P_M, to leucine leads to the loss of the Mg^{2+} and the formation of a $(BChl)_L-(BPhe)_M$ heterodimer (Bylina & Youvan, 1988; Schenck et al., 1990). It has been shown that, due to the different redox potentials of BChl *a* and BPhe *a* (Fajer et al., 1975), the unpaired electron spin density is completely localized on the BChl side in this mutant (Huber et al., 1990). In this study we also examine the effects of the addition or removal of hydrogen bonds to P_L and P_M on the spin density distribution of $P^{\bullet+}$ in this heterodimer.

MATERIALS AND METHODS

Genetic Procedures, Site-Directed Mutagenesis, and DNA Nucleotide Sequencing. The construction of the hydrogen bond mutants LH(L131), LH(M160), HF(L168), and FH-(M197) and the complete set of double mutants has been described in detail (Williams et al., 1992a,b; Murchison et al., 1993; Lin et al., 1994b).

Recombinant DNA techniques for the heterodimer + hydrogen bond mutants were performed as described by Sambrook et al. (1989). The mutants were constructed using the vector set described by Paddock et al. (1989) and Williams et al. (1992a). Oligonucleotide-directed mutagenesis was performed using a combination of the methods developed by Kunkel et al. (1987) and Vandeyar et al. (1988) using uracil-containing templates and 5-methyl-dCTP for second strand synthesis together with nicking and exonuclease treatment to select for the mutant strand. Verification of the mutation was done by sequencing both the initial mutation in the M13mp18 clones and the final mutation in the plasmid pRK404 used to complement the *Rb. sphaeroides* deletion mutant DLM.1 (Paddock et al., 1989). DNA sequencing was performed using the dideoxy procedure of Sanger et al. (1977).

RC Isolation. For all experiments, wild-type reaction centers of *Rb. sphaeroides* were those isolated from the deletion strain complemented with the wild-type genes as described in Williams et al. (1992a). The complemented *Rb. sphaeroides* mutant strains were grown semianaerobically in the dark. The purification of the RCs followed the procedures described by Feher and Okamura (1978) with slight modifications. The cells were resuspended in 15 mM Tris-HCl and 1 mM EDTA, pH 8 (TE), and disrupted by ultrasonification. Solubilization and first ammonium sulfate precipitation leading to a floating pellet were carried out as described by Feher and Okamura (1978). The floating pellet was resuspended in TE buffer and clarified by centrifugation. The solution was dialyzed against TE with 0.1% LDAO (TEL). Deviating from the method of Feher and Okamura (1978), no Celite step was used. For the final purification of the RCs, the sample was applied to a TSK DEAE 650 column and washed with approximately 20 column volumes of TLE containing 30 mM NaCl. RCs were eluted by a gradient from 30 to 250 mM NaCl in TLE. The RC fractions were dialyzed against TLE. The ratio of the absorbance at 280/802 nm was between 1.2 and 1.4 for all RC preparations used in this study. For the EPR and ENDOR measurements, all mutant RCs were concentrated to an absorbance of A_{802}^{1cm} between 70 and 100. Chromatophores of the mutants were concentrated to $A_{865}^{1cm} = 150$.

EPR and ENDOR Spectroscopy. The EPR, ENDOR, and TRIPLE spectra were recorded using a Bruker ESP 300E spectrometer equipped with home-built ENDOR/TRIPLE accessories as previously descibed (Rautter et al., 1994). For EPR measurements a standard rectangular cavity (Bruker ER 4102 ST) was used. All ENDOR and TRIPLE experiments were performed with a TM_{110} cavity of local design similar to the one described in Zweygart et al. (1994) attached to a Bruker ER 4111 VT nitrogen gas cooling system for temperature control of the sample (100−300 K).

For experiments on RCs in liquid solution capillaries of 1 mm inner diameter were used to minimize dielectric losses. The cation radical of the primary donor was generated by *in situ* illumination of the RCs in the range of 830−900 nm at 288 K with a 100 W tungsten halogen lamp. The RC and chromatophore samples for the frozen solution measurements were prepared in quartz tubes (i.d. 3mm) with 65% (v/v) glycerol as cryoprotectant for the RCs to avoid changes in the spin density distribution that have been observed when freezing unprotected *Rb. sphaeroides* R-26 RCs (Käss et al., 1995). The samples were illuminated for 10−20 s, under the same light conditions as above, prior to freezing in liquid nitrogen.

For measuring the proton hfcs of $P^{\bullet+}$ in liquid solutions, Special TRIPLE resonance, an extension of ENDOR spectroscopy, has been applied. In this experiment both the low- and high-frequency ENDOR transitions of a set of equivalent protons with the isotropic hyperfine coupling constant *a* that are symmetrically spaced about the proton Larmor frequency ν_H

$$\nu_{ENDOR} = |\nu_H \pm \frac{a}{2}| \quad (1)$$

are induced simultaneously. This is achieved by sweeping two side-bands symmetrically about ν_H. In this way the signal amplitudes become independent from the limiting nuclear relaxation rates and are generally larger than in the ENDOR experiment. The Special TRIPLE frequency axis

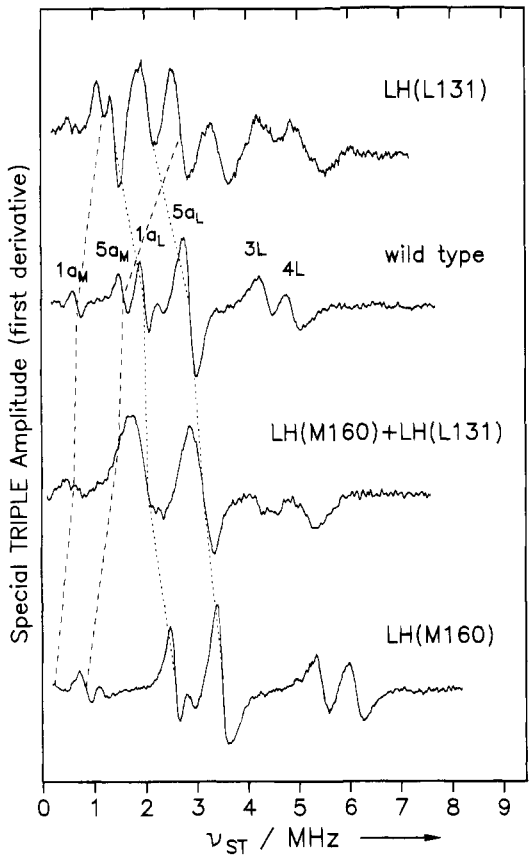

FIGURE 3: Comparison of the ^{1}H Special TRIPLE spectra of $P^{\bullet+}$ in RCs of mutants in the vicinity of the 9-keto groups of the primary donor with that of the wild type. For *Rb. sphaeroides* wild type the assignment of spectral lines (hfcs) to molecular positions is given (for numbering, see Figure 1). The change of line positions for $P^{\bullet+}$ in the mutant RCs with respect to the wild type is indicated by dashed ($1a_M$, $5a_M$) and dotted lines ($1a_L$, $5a_L$) (see text). Experimental conditions: T = 288 K; rf power, 2 × 150 W; microwave power, 10−20 mW; rf modulation depth, 150 kHz (frequency 12.5 kHz); accumulation times, 1−3 h.

gives the deviation from ν_H, and the line positions correspond to half of the respective hfc.

The relative signs of hfcs can be obtained employing general TRIPLE resonance [for reviews, see Kurreck et al. (1988), Möbius et al. (1989), and Lubitz (1991)]. In the general TRIPLE experiment one specific NMR transition is pumped with the respective (unmodulated) rf frequency, while the ENDOR spectrum is recorded. Only the lines of transitions belonging to the same manifold as the one that is pumped show intensity changes when compared with the normal ENDOR experiment. Therefore, this technique can be also be used to assign lines in a spectrum to different species of RCs. For the evaluation of spectra with overlapping lines a spectral deconvolution program was employed (Tränkle & Lendzian, 1989).

RESULTS

The Special TRIPLE spectrum of $P^{\bullet+}$ in the deletion strain of *Rb. sphaeroides* complemented with the wild type genes is shown in Figure 3. This spectrum is identical (within experimental errors) with that of the wild-type 2.4.1 and very similar (the hfcs agree within 3%) to that of $P^{\bullet+}$ in RCs of the carotenoidless strain R-26 (Gessner et al., 1992). For the wild-type 2.4.1 and R-26 most hfcs of $P^{\bullet+}$ have been unambigously assigned by experiments performed on RC single crystals (Gessner et al., 1992; Lendzian et al., 1993). The assignment of the four lines of the methyl protons at positions 1a and 5a in P_L and P_M is indicated in Figure 3. The analysis of the spectra from the RC single crystals yielded an asymmetric distribution of π-spin density of approximately 2:1 in favor of the L-half of the primary donor. The largest coupling constants in BChl $a^{\bullet+}$ as well as in the moieties P_L and P_M of $P^{\bullet+}$, result from the β-protons at rings II and IV and the methyl protons in positions 1a and 5a (these protons are indicated by shaded circles in Figure 1). Since the β-proton hfcs at positions 3, 4, 7, and 8 are strongly dependent on the geometry of the respective hydrated rings II and IV, they are not very well suited for probing the π-spin density of the macrocycle (Käss et al., 1994). The methyl protons 1a and 5a are better probes of the spin density distribution since their isotropic hfcs are directly proportional to the π-spin density on the neighboring carbon atom in the macrocycle. Due to the rotation of the methyl group, all three protons are equivalent and exhibit only one hfc. The lines belonging to these groups are indicated in Figure 3 for the respective dimer halves P_L and P_M. The identification of the hfcs of the methyl protons of $P^{\bullet+}$ in all mutants was achieved by a comparison between liquid and frozen solution spectra (data not shown). In contrast to other β-protons, the methyl protons exhibit relatively sharp and intense lines in frozen solution due to the small anisotropy and the free rotation of the methyl groups even at low temperatures (Hyde et al., 1968; Feher et al., 1975). For $P^{\bullet+}$ in the hydrogen bond mutants the hfcs belonging to the four methyl groups of $P^{\bullet+}$ could all be identified (see Tables 1−3).

It is important to note that in the Special TRIPLE spectra of liquid RC solutions the relative line intensities do not reflect the relative number of contributing nuclei. Instead, all line intensities decrease considerably toward smaller frequencies. This is caused by a nonselective EPR-saturation of neighboring transitions for small hfcs (Allendoerfer & Maki, 1970) and can be cleary observed for the four resolved methyl proton hfcs in the wild-type spectrum of Figure 3.

An individual assignment of the observed hfcs to the specific molecular positions in P_L and P_M of the various mutants could not be obtained directly since single crystals of the mutant RCs large enough for ENDOR measurements are not yet available. An assignment of the methyl protons is, however, possible since the methyl proton hfcs A at positions 1a and 5a exhibit characteristic ratios for the L and M halves of the dimer in *Rb. sphaeroides* (Feher, 1992). This is due to the different geometries of the BChl *a* molecules constituting the dimer. These ratios are $A(5a)/A(1a) = 1.44$ for P_L and $A(5a)/A(1a) = 2.35$ for P_M in the wild type (see Table 1). Our assignment of the methyl protons of P_L and P_M given in the tables is based on the assumption that these ratios do not change significantly in the investigated mutant RCs. The variation of these ratios in the different mutants is considerably smaller than the large difference in ratios between P_L and P_M (see Table 1). In all investigated mutants two methyl line pairs are found which have approximately the above mentioned ratios of corresponding hfcs. Furthermore, the sum of all methyl proton hfcs is constant within 5% in all mutants. This indicates that no significant redistribution of spin density occurs within the macrocycles of P_L and P_M. Identical spin density

Table 1: ^{1}H hfcs (MHz), Ratios of hfcs, and EPR Line Widths of $P^{\bullet+}$ in the Investigated RCs of the Mutants in the Vicinity of the 9-Keto Groups and for Wild Type[a] of *Rb. sphaeroides*

	$P^{\bullet+}$			
	LH(M160)	LH(L131)	LH(M160) + LH(L131)	wild type[a]
$A(5a_L)$[b]	6.95	3.98	6.10	5.75
$A(1a_L)$	5.15	2.87	3.97	3.98
$A(5a_M)$	1.70	5.42	3.19	3.24
$A(1a_M)$	0.75[c]	2.33	1.37	1.38
β_L[d]	12.20	10.30[e]	10.05	9.75
	10.90	8.85	8.45	8.75
	7.95	6.90	7.00	6.75
	5.60	6.00		
β_M[d]		4.50	4.65	4.60
$[A(5a)/A(1a)]_L$[f]	1.35	1.38	1.54	1.44
$[A(5a)/A(1a)]_M$[f]	2.27	2.33	2.36	2.35
$\sum A(CH_3)$	14.60	14.60	14.63	14.35
$\sum A(CH_3)_L/[\sum A(CH_3)_L + \sum A(CH_3)_M]$[g]	0.83	0.47	0.69	0.68
ΔB_{pp} (mT) exp[h]	1.09 ± 0.02	0.98 ± 0.03	0.97 ± 0.02	0.96 ± 0.02
ΔB_{pp} (mT) sim[i]	1.08	0.97	0.96	0.95

[a] Wild-type RCs are those of the deletion strain reconstructed with the wild-type genes. Errors of hfcs are ±20 kHz for methyl protons (1a and 5a) and ±50 kHz for β-protons (valid for all mutants). [b] For numbering of positions, see Figure 1; for assignments, see text. [c] This methyl hfc was derived from the frozen solution ENDOR spectrum. [d] Only the largest, clearly resolved β-proton hfcs at rings II and IV (Figure 1) assigned to P_L or P_M, depending on the spin density fraction, are given. In the range of smaller couplings (≤5 MHz) several additional lines were resolved, which were tentatively assigned to β-protons of rings II and IV of the respective half with the smaller spin density fraction (see text). [e] Due to the nearly symmetric spin density distribution over the two dimer halves, an assignment of these couplings to individual moieties in LH(L131) is not feasible. [f] Errors for hfc ratios: ±2%. [g] Fraction of spin density on P_L as measured from the CH_3 hfcs at positions 1a and 5a. [h] Experimental peak-to-peak Gaussian envelope EPR line width. [i] Simulated EPR line width using the hfcs from ENDOR (for details see text).

Table 2: ^{1}H hfcs (MHz), Ratios of hfcs, and EPR Line Widths of $P^{\bullet+}$ in the Investigated RCs of the Mutants in the Vicinity of the 2-Acetyl Groups and for Wild Type[a] of *Rb. sphaeroides*

	$P^{\bullet+}$			
	FH(M197)	HF(L168)	HF(L168) + FH(M197)	wild type[a]
$A(5a_L)$[b]	5.43	3.31	3.32	5.75
$A(1a_L)$	4.05	2.65	2.65	3.98
$A(5a_M)$	3.45	5.59	5.72	3.24
$A(1a_M)$	1.74	2.28	3.04	1.38
β_L[c]	9.20	10.65[d]	11.30[d]	9.75
	7.95	9.35	9.75	8.75
	5.75	7.15	7.80	6.75
		6.30	6.50	
β_M[c]	4.65	4.95	4.85	4.60
$[A(5a)/A(1a)]_L$[e]	1.34	1.25	1.25	1.44
$[A(5a)/A(1a)]_M$[e]	1.98	2.45	1.88	2.35
$\sum A(CH_3)$	14.67	13.83	14.73	14.35
$\sum A(CH_3)_L/[\sum A(CH_3)_L + \sum A(CH_3)_M]$[f]	0.65	0.43	0.41	0.68
ΔB_{pp} (mT) exp[g]	0.95 ± 0.02	0.97 ± 0.02	1.00 ± 0.02	0.96 ± 0.02
ΔB_{pp} (mT) sim[g]	0.93	0.96	0.99	0.95

[a] Wild-type RCs are those of the deletion strain reconstructed with the wild type genes. Errors of hfcs: ±20 kHz for methyl protons (1a and 5a); ±50 kHz for β-protons (valid for all mutants). [b] For numbering of positions see Figure 1; for assignments see text. [c] Only the largest, clearly resolved β-proton hfcs at rings II and IV (Figure 1) assigned to P_L or P_M, depending on the spin density fraction, are given. In the range of smaller couplings (≤5 MHz) several additional lines were resolved, which were tentatively assigned to β-protons of rings II and IV of the respective half with the smaller spin density fraction (see text). [d] Due to the nearly symmetric spin density distribution over the two dimer halves, an assignment of these couplings to individual moieties in HF(L168) is not feasible. [e] Errors for hfc ratios: ±2%. [f] Fraction of spin density on P_L as measured from the CH_3 hfcs 1a and 5a. [g] Experimental and simulated peak-to-peak Gaussian envelope EPR line width.

distributions were measured for $P^{\bullet+}$ in isolated RCs and in chromatophores for all mutants (data not shown).

Mutations in the Vicinity of the 9-Keto Groups. Figure 3 shows the spectra of the mutants designed to introduce hydrogen bonds to the 9-keto groups of the primary donor, namely, LH(M160), LH(L131), and the double mutant LH(M160) + LH(L131) (cf. Figure 2), together with that of the wild type of *Rb. sphaeroides*.

In the spectrum of $P^{\bullet+}$ in RCs of LH(M160) two large and one small methyl hfcs are detected. On the basis of the assumptions stated above, the large methyl hfcs of 6.95 MHz and 5.15 MHz were assigned to positions 5a and 1a of P_L (see Table 1). The ratio of the small methyl hfc of 1.70 MHz in Figure 3 and the fourth methyl hfc of 0.75 MHz, which is obtained from the frozen solution ENDOR spectrum of LH(M160) (Rautter et al., 1992), is 2.27, which leads to an assignment of these hfcs to positions 5a and 1a in P_M. This reveals a strongly asymmetric distribution of the unpaired electron in $P^{\bullet+}$ of LH(M160) with 83% of the spin density on P_L as compared with the wild type, which has 68% of the spin density on P_L. It should be noted that the spectrum of LH(M160) is quite similar to that of the heterodimer HL(M202) where the unpaired electron resides on the L-half BChl *a* of $P^{\bullet+}$ (Huber et al., 1990). Our spectrum of $P^{\bullet+}$ in this mutant is shown in Figure 6. The β-proton hfcs of LH(M160), given in Table 1, are assigned

Table 3: ^{1}H hfcs (MHz), Ratios of hfcs, and EPR Line Widths of $P^{\bullet+}$ in the Investigated RCs of Double Mutants of *Rb. sphaeroides*

	$P^{\bullet+}$			
	LH(M160) + FH(M197)	LH(M160) + HF(L168)	LH(L131) + FH(M197)	LH(L131) + HF(L168)
$A(5a_L)$[a]	7.15	5.92	3.68	1.88
$A(1a_L)$	5.31	4.35	2.43	1.26
$A(5a_M)$	1.86	3.07	5.69	7.51
$A(1a_M)$	0.70[b]	1.32	3.35	3.83
β_L[c]	12.10	10.20	4.95	
	10.55	8.20		
	7.60			
	5.90			
β_M[c]			11.10	14.25
			10.05	12.95
			9.10	9.30
			6.90	7.05
$[A(5a)/A(1a)]_L$[d]	1.35	1.36	1.51	1.49
$[A(5a)/A(1a)]_M$[d]	2.66	2.33	1.70	1.96
$\Sigma A(CH_3)$	15.02	14.66	15.15	14.48
$\Sigma A(CH_3)_L/[\Sigma A(CH_3)_L + \Sigma A(CH_3)_M]$[e]	0.83	0.70	0.40	0.22
ΔBpp (mT) exp[f]	1.10 ± 0.02	*g*	1.02 ± 0.02	1.12 ± 0.02
ΔBpp (mT) sim[f]	1.10	*g*	1.01	1.12

[a] For numbering of positions see Figure 1; for assignments see text. [b] This methyl hfc was derived from the frozen solution ENDOR spectrum. [c] Only the largest, clearly resolved β-proton hfcs of rings II and IV (Figure 1) assigned to P_L or P_M, depending on the spin density fraction, are given. In the range of smaller couplings (≤5 MHz) several additional lines were resolved, which were tentatively assigned to β-protons of rings II and IV of the respective half with the smaller spin density fraction (see text). [d] Errors for hfc ratios: ±2%. [e] Fraction of spin density on P_L as measured from the CH_3 hfcs 1a and 5a. [f] Experimental and simulated peak-to-peak Gaussian envelope EPR line width. [g] Due to the presence of a second species and its contribution to the EPR line width, no values are given for this mutant.

Table 4: ^{1}H hfcs (MHz), Ratios of hfcs of $P^{\bullet+}$ in the RCs of the Combined Heterodimer, and Hydrogen Bond Mutants of *Rb. sphaeroides*

	$P^{\bullet+}$			
	wild type[a]	HL(M202)	HL(M202) + HF(L168)	HL(M202) + LH(L131)
$A(5a)_L$[b]	5.75	7.44	7.40	8.22
$A(1a_L)$	3.98	5.75	5.24	5.68
	9.75	13.70	13.65	13.85
β_L	8.75	12.45	11.45	12.25
	6.75	8.10	7.85	8.80
		6.25	5.80	
$[A(5a)/A(1a)]_L$[c]	1.44	1.29	1.41	1.45
$\Sigma A(CH_3)$	14.35	13.19	12.64	13.96
ΔBpp (mT) exp[d]	0.96 ± 0.02	1.22 ± 0.02	1.20 ± 0.02	1.23 ± 0.03

[a] Wild-type RCs are those of the deletion strain reconstructed with the wild-type genes. [b] For numbering of positions see Figure 1; for assignments see text. [c] Errors for hfc ratios ±2%. [d] Experimental peak-to-peak Gaussian envelope EPR line width.

to P_L in analogy to the wild type and the HL(M202) heterodimer (Table 4), because only the protons of P_L contribute to this region of the spectrum.

In LH(L131) (Figure 3) four methyl group hfcs of comparable magnitude are detected, pointing to a more symmetric spin density distribution in $P^{\bullet+}$. On the basis of the assumption that the ratios of the methyl couplings 5a versus 1a are also conserved in this mutant, the hfcs of 5.42 and 2.33 MHz were assigned to 5a and 1a of P_M and the couplings of 3.98 and 2.87 MHz were assigned to the respective positions in P_L (see Table 1). This corresponds to an almost symmetric spin density distribution over the two dimer halves with a slight excess (53%) on P_M. Because of the high symmetry of this state, an assignment of the additionally observed hfcs of the β-protons at rings II and IV, given in Table 1, to the individual dimer halves is not possible. The two mutations LH(M160) and LH(L131) cause significant spin density shifts within $P^{\bullet+}$ in opposite directions. The spectrum of the double mutant LH(L131) + LH(M160) (see Figure 3) exhibits two prominent lines near 3.0 MHz and around 2 MHz. The line around 2 MHz in the spectrum of LH(L131) + LH(M160) has a large relative intensity compared with the lines in the wild type observed at comparable frequencies because it consists of two lines of almost equal intensity, as inferred by spectral deconvolution. The overall appearance of this spectrum is similar to that of the wild type except for the larger linewidths. The assignment of the hfcs of the methyl couplings to P_L and P_M based on the ratio of the methyl hfcs (see Table 1) yields a spin density distribution with 69% of the unpaired electron on P_L. This is close to the value for the wild type and shows that the effects of the two mutations compensate each other with respect to the spin density distribution. The obtained hfcs, ratios of the methyl proton hfcs, and the deduced spin density ratios are collected in Table 1.

Mutations in the Vicinity of the 2-Acetyl Groups. In Figure 4 the Special TRIPLE spectra of $P^{\bullet+}$ in mutants designed to add or remove hydrogen bonds to the 2-acetyl group oxygens of the primary donor, HF(L168), FH(M197), and the double mutant HF(L168) + FH(M197) are shown, together with that of the wild type. The lines belonging to methyl groups were identified by ENDOR on RCs in frozen solutions (data not shown). The spectrum of $P^{\bullet+}$ in the mutant HF(L168), in which the only existing hydrogen bond between the protein and a carbonyl group of P is cleaved, shows the largest methyl line near 2.8 MHz and several overlapping lines between 1 and 2 MHz with a large integral intensity compared with the lines in the same frequency range in the wild type. Spectral deconvolution shows that this region consists of three lines of almost equal line width and intensity, which are assigned to the other three methyl group hfcs. The assignment of the four methyl couplings to the individual dimer halves is based on the assumption of conserved ratios of the methyl hfcs as described above. This leads to a nearly symmetric spin density distribution, with 57% of the spin density on P_M (see Table 2). An assignment of the β-protons to P_L or P_M is difficult for HF(L168). This

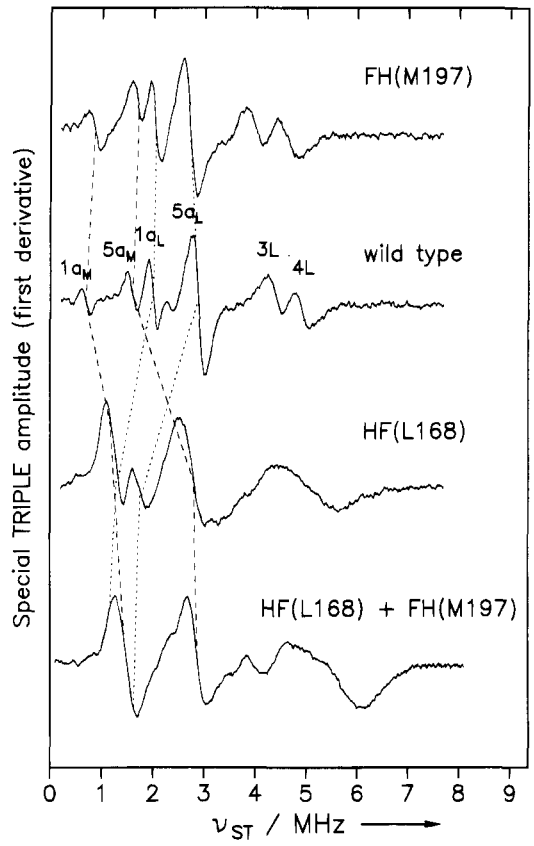

FIGURE 4: Comparison of the ^{1}H Special TRIPLE spectra of $P^{\bullet+}$ in RCs of mutants in the vicinity of the 2-acetyl groups of the primary donor with that of the wild type. For *Rb. sphaeroides* wild type the assignment of spectral lines (hfcs) to molecular positions is given (for numbering, see Figure 1). The change of line positions for $P^{\bullet+}$ in the mutant RCs with respect to the wild type is indicated by dashed ($1a_M$, $5a_M$) and dotted lines ($1a_L$, $5a_L$) (see text). For experimental conditions, see the legend to Figure 3.

was also found for the other mutant LH(L131) with a more symmetric spin density distribution.

At first glance, the Special TRIPLE spectrum of $P^{\bullet+}$ in the mutant FH(M197) looks very similar to that of the wild type (Figure 4). The two large methyl hfcs of 5.43 and 4.05 MHz were assigned to positions 5a and 1a of P_L and the two small hfcs of 3.45 MHz and 1.74 MHz to positions 5a and 1a of P_M. This corresponds to 65% of the spin density on P_L, which is very similar to the value in the wild type (68%). The most pronounced difference is the changed ratio of the methyl couplings on P_M, $A(5a)/A(1a) = 1.98$ which is 2.35 in the wild type (Table 2). The Special TRIPLE spectrum of the double mutant HF(L168) + FH(M197) is dominated by two lines of large integral intensity and looks similar to that of HF(L168). The large methyl coupling of 5.72 MHz is comparable to that of HF(L168). The line at approximately 1.5 MHz has an even larger integral intensity than the strong line in the spectrum of HF(L168) and a deconvolution yields three lines of almost equal intensity which are assigned to the remaining three methyl groups. This assignment leads to a similar spin density distribution as in HF(L168) with 59% of the spin on P_M (Table 2). In this mutant the ratio of the methyl couplings on P_M is also smaller (1.88) than in the wild type (2.35). The spectrum of the double mutant HF(L168) + FH(M197) is consistent with a superposition of the observed effects for the respective single mutants.

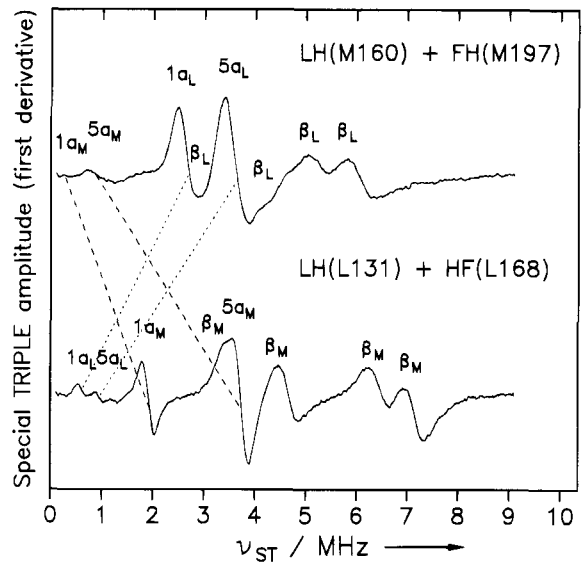

FIGURE 5: Comparison of the ^{1}H Special TRIPLE spectra of $P^{\bullet+}$ in RCs of two of the double mutants that combine the mutations near the 2-acetyl and 9-keto groups of the primary donor. The assignment of lines belonging to methyl hfcs of $P^{\bullet+}$ (for numbering, see Figure 1) is given by dashed ($1a_M$, $5a_M$) and dotted lines ($1a_L$, $5a_L$) (see text). Experimental conditions: $T = 288$ K; rf power, 2 × 150 W; microwave power, 10 mW; rf modulation depth, 150 kHz (frequency 12.5 kHz); accumulation times, 1 h.

Combined Double Mutations. Figure 5 shows the Special TRIPLE spectra of $P^{\bullet+}$ in two of the double mutants which combine hydrogen-bond changes to the 9-keto group and the 2-acetyl group. In the spectrum of $P^{\bullet+}$ of LH(M160) + FH(M197), three methyl group hfcs can be identified. The two large methyl hfcs of 7.15 and 5.31 MHz were assigned to position 5a and 1a of P_L on the basis of their ratio (1.35, see Table 3). The smallest methyl hfc of 0.70 MHz was obtained from the respective frozen solution spectrum (data not shown). Together with the small methyl coupling of 1.86 MHz detected in the Special TRIPLE spectrum, this gives a ratio of $A(5a)/A(1a)$ of 2.66 for P_M. This leads to a spin density distribution with 83% of the unpaired electron residing on P_L, which is very similar to the single mutant LH(M160).

In the double mutant LH(L131) + HF(L168) the Special TRIPLE spectrum of $P^{\bullet+}$ shows two large methyl lines that correspond to hfcs of 7.51 and 3.83 MHz. On the basis of their ratio of 1.96, these methyl couplings are assigned to the dimer half P_M. The two small methyl hfcs of 1.88 and 1.26 MHz yield a ratio of 1.49 and are assigned to P_L. This gives an asymmetric spin density distribution with 78% of the unpaired electron on P_M. The observed large β-proton hfcs of 14.25 and 12.95 MHz are also assigned to P_M. It is known from experiments on the heterodimers HL(M202) and HL(L173) (Huber et al., 1990) that the M-half BChl exhibits larger β-proton hfcs—as compared to the methyl couplings—than the L-half BChl. This effect is observed in all mutants with an excess of spin density on P_M (see Tables 1−3). The two mutants demonstrate the large changes of the spin density distribution of $P^{\bullet+}$ caused by altering the number of hydrogen bonds to the primary donor. The two other double mutants LH(M160) + HF(L168), with 70% of the spin density on P_L, and LH(L131) + FH(M197), with 60% of the spin density on P_M, represent intermediate cases (see Table 3).

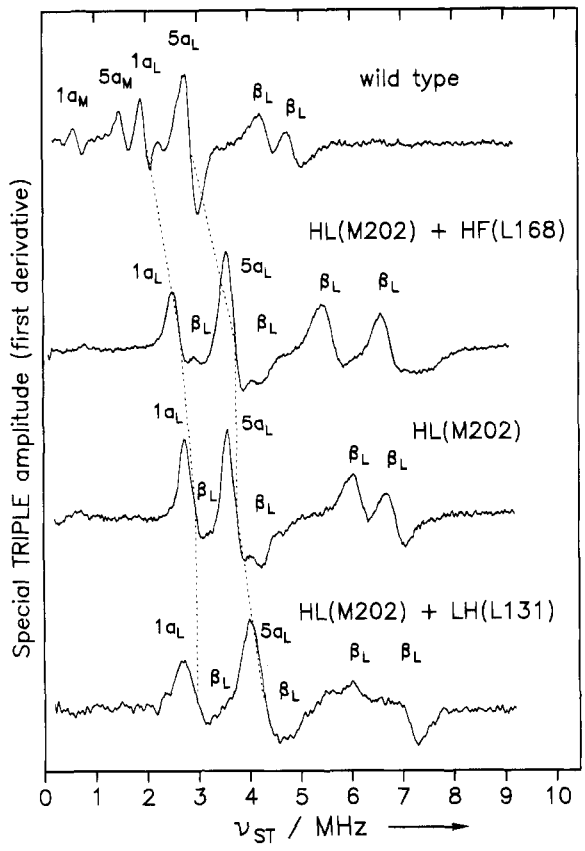

FIGURE 6: Comparison of the ^{1}H Special TRIPLE spectra of $P^{\bullet+}$ in RCs of the double mutants that form hydrogen bonds to the primary donor of the heterodimer HL(M202) with that of the wild type and of HL(M202). For *Rb. sphaeroides* wild type the assignment of spectral lines (hfcs) to molecular positions is given (for numbering, see Figure 1). The change of line positions for $P^{\bullet+}$ in the mutant RCs with respect to the wild type is indicated by dotted lines ($1a_L$, $5a_L$) (see text). For experimental conditions, see the legend to Figure 3 (accumulation time between 1 and 5 h for each spectrum).

Influence of Different Hydrogen Bonds to $P^{\bullet+}$ in Double Mutants Containing the Heterodimer Mutation HL(M202). In order to investigate the effects of the formation and removal of the hydrogen bonds on P_L, we have investigated the heterodimer HL(M202), which is known to have the unpaired electron localized on the L-half BChl (Huber et al., 1990), and combinations of this mutation with the two hydrogen bond mutations that directly affect the L-half, i.e., HF(L168) and LH(L131).

Figure 6 shows the Special TRIPLE spectra of $P^{\bullet+}$ in the double mutants HL(M202) + HF(L168) and HL(M202) + LH(L131) together with that of HL(M202) and the wild type in liquid RC solution. The obtained hfcs for the heterodimer HL(M202) (see Table 4) are in good in agreement (within 3%) with those reported by Huber et al. (1990) with the exception that we assign the two shoulders near the methyl lines to the smaller β-proton hfcs of P_L as infered by spectral deconvolution, whereas Huber et al. (1990) assigned all four β-protons to the two lines at the highest frequency.

The spectra of the double mutants HL(M202) + HF(L168) and HL(M202) + LH(L131) look similar to that of the heterodimer HL(M202) with some small differences. The spectrum of HL(M202) + HF(L168) is dominated by the two large methyl hfcs of 7.40 and 5.24 MHz. The ratio of these two methyl hfcs is 1.41, as compared to 1.29 in HL(M202). This shows that the ratio of the methyl hfcs on the L-half is only slightly changed due to the reorientation of the 2-acetyl group caused by the loss of the hydrogen bond to the amino acid residue L168. In addition, all four hfcs of the β-protons of the hydrated rings II and IV of P_L are observed. The two smaller hfcs appear as shoulders of the methyl lines and can be resolved via spectral deconvolution (see Table 4). The changes of the β-proton hfcs indicate small geometrical changes of the saturated rings II and IV in this mutant. The Special TRIPLE spectrum of HL(M202) + LH(L131) shows two large methyl hfcs of 8.22 MHz and 5.68 MHz (ratio 1.45; see Table 4) and four β-protons of the hydrated rings II and IV which are also assigned to P_L.

In both double mutants no small methyl hfcs could be detected, which indicates a complete localization of the unpaired electron on the L-half BChl. All assignments of the methyl proton hfcs in the investigated mutants depend on the different ratios of the methyl hfcs 5a versus 1a for the two dimer halves P_L and P_M. The results for the combined heterodimer and hydrogen bond mutants confirm that changes in the hydrogen bonding of P_L have only a minor influence on that ratio and the assignment of the methyl couplings to the respective dimer half in the various hydrogen bond mutants (see above) is justified.

To investigate if the formation of hydrogen bonds to the M-half BPhe leads to changes in the spin density distribution of the radical cation of the heterodimer, the double mutants HL(M202) + LH(M160) and HL(M202) + FH(M197) were also constructed. Since these two double mutants exhibit a 5 times lower quantum yield for the formation of $P^{\bullet+}$ compared to HL(M202), measurements in liquid RC solution were not feasible. Figure 7 shows a comparison of the ENDOR spectra of all four double mutants with HL(M202) in frozen solution at 160 K (solid lines). In these spectra only the two large methyl hfcs are observed. The spectra were simulated (dotted lines) using axially symmetric methyl hfc tensors with the values given in Table 5. For HL(M202) the obtained values (see Table 5) are in good agreement with those reported by Huber et al. (1990).

The isotropic values calculated from the methyl tensors of HL(M202) + HF(L168) and HL(M202) + LH(L131) (see Table 5) are in good agreement with those obtained in liquid solution (see Table 4). The comparison of the spectra for HL(M202), HL(M202) + LH(M160), and HL(M202) + FH(M197) reveals no changes of the spin density distribution of $P^{\bullet+}$ due to the additional hydrogen bonds to the BPhe at P_M (see Table 5).

EPR Spectra. The EPR spectra of all the investigated mutants consist of Gaussian envelopes with no resolved hyperfine structure. In the series of the hydrogen bond mutants only the single mutant LH(M160) and the two double mutants LH(M160) + FH(M197) and LH(L131) + HF(L168) exhibit a significant increase in the EPR line width as compared to wild type. Their respective measured line widths of ΔB_{pp} of 1.09 ± 0.02, 1.10 ± 0.02, and 1.12 ± 0.02 mT already point toward a more asymmetric distribution of the unpaired electron. For the relation between EPR line width and spin density asymmetry in a dimer see Lendzian et al. (1993), Appendix A. All other single and double mutants show line widths that are comparable to the value of (0.96 ± 0.02 mT) for the wild type (spectra not shown;

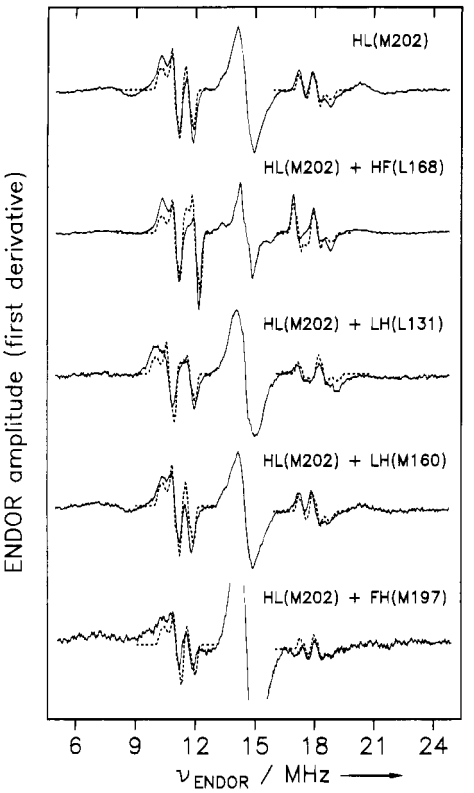

FIGURE 7: Comparison of the ENDOR spectra of $P^{\bullet+}$ in RC's of the combination of the heterodimer and the hydrogen bond mutations together with HL(M202) in frozen solution with 67% (v/v) glycerol as cryoprotectant. Experimental spectra (solid lines) are shown with simulations employing axially symmetric hfc tensors (see Table 5) for the methyl protons (dotted lines). Experimental conditions: T = 160 K; rf power, 200 W; microwave power, 5 mW; rf modulation depth, 200 kHz (frequency 12.5 kHz); accumulation times, 1−4 h.

Table 5: Comparison of Methyl Proton hfc Tensor Principal Values (MHz) for $P^{\bullet+}$ in RCs of the Combined Heterodimer and Hydrogen Bond Mutants of *Rb. sphaeroides*[a]

	$P^{\bullet+}$					
	methyl group $5a_L$[b]			methyl group $1a_L$[b]		
mutant species	$A_\perp$	$A_\parallel$	A_{iso}	$A_\perp$	$A_\parallel$	A_{iso}
HL(M202)	7.0	8.7	7.6	5.6	6.8	6.0
HL(M202) + HF(L168)	7.0	8.7	7.6	5.0	6.3	5.4
HL(M202) + LH(L131)	7.7	9.3	8.2	5.5	6.8	5.9
HL(M202) + LH(M160)	7.0	8.6	7.5	5.6	6.8	6.0
HL(M202) + FH(M197)	7.0	8.6	7.5	5.6	6.8	6.0

[a] Frozen solution, T = 160 K. [b] Principal values $A_\parallel$ and $A_\perp$ obtained from simulations of the ENDOR spectra (Figure 7) assuming axially symmetric hfc tensors, $A_{iso} = (2A_\perp + A_\parallel)/3$.

see Table 1−3). The combinations of the hydrogen bond and heterodimer mutations exhibit EPR line widths comparable to that of the heterodimer alone, ranging from 1.20 to 1.23 mT (see Table 4).

EPR simulations of the spectra have been performed for the wild type and all mutants, using the hfcs and assignments given in Tables 1−4. The remaining small ^1H hfcs that are not resolved in the ENDOR and Special TRIPLE spectra, and the ^{14}N hfcs were estimated for P_L and P_M by scaling the respective values of BChl $a^{\bullet+}$ (Lubitz, 1991) with the spin density ratios given in Tables 1−3. For all mutants the respective simulated spectra agree well with the observed ones.

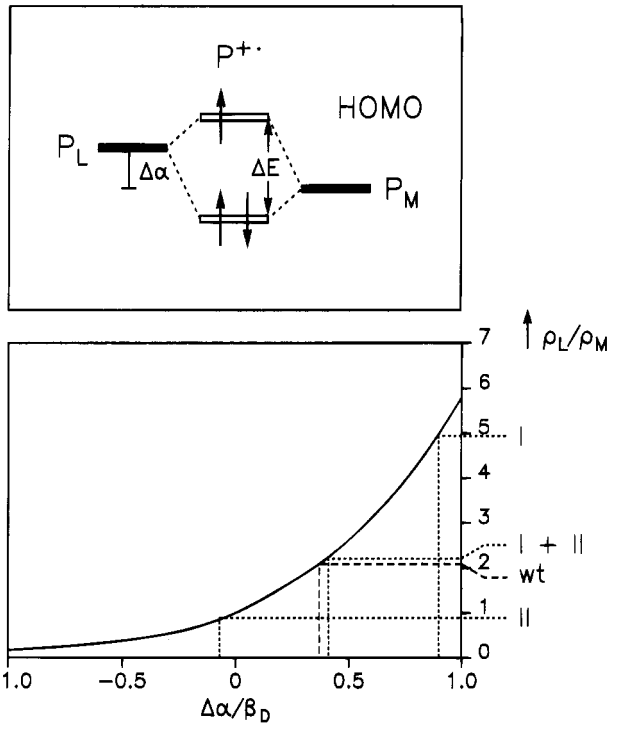

FIGURE 8: (Top) Energy level scheme showing the HOMOs of the monomeric halves P_L and P_M of the dimer and the two supermolecular orbitals. $\Delta\alpha$ is the difference of the Coulomb energies of P_L and P_M; β_D is the resonance integral between P_L and P_M (see text). ΔE is the energy difference between the two supermolecular orbitals (see eq 2). (Bottom) Relation between the ratios of the sums of spin densities ϱ_L/ϱ_M and the ratio $\Delta\alpha/\beta_D$ of a model dimer obtained from a HMO calculation (Plato et al., 1992). The ratios ϱ_L/ϱ_M for $P^{\bullet+}$ in the RCs of the mutants in the vicinity of the 9-keto group are given as an example (dottet lines) together with that of the wild type (wt, dashed lines). (I) LH(M160); (II) LH(L131); (I + II) LH(M160) + LH(L131).

DISCUSSION

The large shifts of spin densities between the dimer halves P_L and P_M in the single and double mutants that alter the hydrogen bonding situation in *Rb. sphaeroides* can be understood on the basis of a dimer model that assumes energetically different orbitals for P_L and P_M. Such dimer models were proposed by Parson et al. (1992) with the emphasis on optical transitions of the primary donor and Plato et al. (1992) to explain the asymmetry of the spin density distribution within $P^{\bullet+}$. The parameters influencing the asymmetry of the spin density distribution are (i) the difference of the Coulomb energies, $\Delta\alpha$ of the highest occupied molecular orbitals (HOMOs), of the two dimer halves P_L and P_M and (ii) the resonance integral, β_D, that is a measure of the strength of the interaction between the two dimer halves (see Figure 8A). Figure 8B shows the spin density ratio as a function of $\Delta\alpha/\beta_D$ obtained from a HMO calculation for an ethylene model dimer (Plato et al., 1992). Applications of this model were already given in Lendzian et al. (1993) for *Rb. sphaeroides* R-26 and in Rautter et al. (1994) for three other purple bacteria. Adapting this model for $P^{\bullet+}$ of *Rb. sphaeroides* R-26 and using the experimental spin density ratio $\varrho_L/\varrho_M \approx 2{:}1$, this yields a value of $\Delta\alpha/\beta_D = 0.37$ without any further assumptions about the magnitude of $\Delta\alpha$ and β_D. The energetic difference ΔE between the

resulting super-MOs of P (see Figure 8) is given in this model by

$$\Delta E = \sqrt{(\Delta\alpha)^2 + (2\beta_D)^2} \quad (2)$$

The energy of this transition in $P^{\bullet+}$ was measured by Breton et al. (1992), who detected an absorption band in the far infrared region at 2600 ± 100 cm^{-1} in RCs from *Rb. sphaeroides*, which corresponds to 322 ± 12 meV. Together with the experimental spin density ratio given above, this yields values of β_D = 160 meV and $\Delta\alpha$ = 55 meV for $P^{\bullet+}$ in *Rb. sphaeroides* R-26 [for details, see Rautter et al. (1994)]. Possible reasons for the different energies of the two BChl *a* moieties are (i) differences in the planarity of the conjugated macrocycles, (ii) different orientations of conjugated substituents, e.g., the 2-acetyl groups, or (iii) asymmetric interactions with the protein environment.

A recent evalution of the crystal structures for seven mutants of *Rb. sphaeroides* showed that no major structural perturbations near the mutation sites occur (Chirino et al., 1994). Even in the mutant HL(M202), the BChl is replaced by BPhe without significant changes of the surrounding protein main-chain or side-chain atoms (Chirino et al., 1994). As was shown by Plato et al. (1992), the deviation of the macrocycles from planarity has only a small effect on the energetic difference of P_L and P_M as compared with the rotation of the conjugated acetyl groups. Rotation (reorientation) of this group is expected in the mutants that form or remove hydrogen bonds to the 2-acetyl group.

In all the investigated mutants the protein−chromophore interactions are specifically altered and the main effects should be changes in the orbital energies (i.e., $\Delta\alpha$) of P_L and P_M. For six of the investigated species ΔE (eq 2) has been measured by IR spectroscopy. For the mutants LH(L131) and the double mutant LH(L131) + LH(M160) the same value as for the wild type (2600 ± 100 cm^{-1}) has been reported (Nabedryk et al., 1993). For the mutants HF(L168) and FH(M197) a small downshift (2570 ± 100 cm^{-1}) was observed (E. Nabedryk, unpublished results). Only mutant LH(M160) showed a substantial shift (2800 ± 100 cm^{-1}). For these mutants both values $\Delta\alpha$ and β_D were calculated as described above for R-26. In all cases β_D remains remarkably constant (157−161 ± 10 meV). Therefore, a constant value of β_D = 160 meV was assumed for *all* mutants in Table 6. For $P^{\bullet+}$ in *Rb. sphaeroides* wild type an energetic difference of $\Delta\alpha$ = 59 meV is obtained (see Table 6), which is slightly different from the value of R-26. This is attributed to the presence of the carotenoid molecule in the RC (Gessner, 1992; Rautter, 1994). The corresponding energetic difference $\Delta\alpha$ in the mutant RCs has to be compared with this value (Table 6).

Mutations in the Vicinity of the 9-Keto Groups. For $P^{\bullet+}$ in the mutant LH(M160) the ratio ϱ_L/ϱ_M is 4.94. This corresponds to $\Delta\alpha/\beta_D$ = 0.90 and, using β_D = 160 meV, yields $\Delta\alpha$ = 144 meV (see Table 6). The large increase of the energetic difference between the two dimer halves of +85 meV in the mutant LH(M160) can be explained by the formation of a hydrogen bond between the histidine introduced at position M160 and the 9-keto group of P_M. The formation of that hydrogen bond lowers the energy of the highest occupied π-orbital (HOMO) of P_M, thereby $\Delta\alpha$ is increased (see Figure 8A).

Table 6: Spin Densities and Energetic Parameters of $P^{\bullet+}$ in the RCs of the Hydrogen Bond Mutants and Wild-type[a] of *Rb. sphaeroides*

mutant	ϱ_L/ϱ_M[b]	$\Delta\alpha/\beta_D$[c]	$\Delta\alpha$ (meV)[d]	$\delta(\Delta\alpha)$ (meV)[e]	E_m (mV)[f]	τ (ns)[g]
HF(L168) + LH(L131)	0.28	−0.7	−112	−167	485	4820
HF(L168) + FH(M197)	0.68	−0.18	−29	−88	545	1515
LH(L131) + FH(M197)	0.68	−0.18	−29	−88	710	165
HF(L168)	0.75	−0.13	−20	−79	410	7730
LH(L131)	0.89	−0.05	−8	−67	565	470
FH(M197)	1.83	0.28	45	−14	630	185
wild type	2.09	0.37	59	0	505	960
LH(M160) + LH(L131)	2.21	0.41	65	+6	635	210
LH(M160) + HF(L168)	2.34	0.43	69	+10	485	1545
LH(M160) + FH(M197)	4.87	0.89	142	+83	700	130
LH(M160)	4.94	0.90	144	+85	565	345

[a] Wild-type RCs are those of the deletion strain reconstructed with the wild-type genes. [b] Ratio of spin densities of the two dimer halves as measured from the CH_3 hfcs at positions 1a and 5a (see Tables 1−3). [c] Ratio of the difference of the Coulomb energies of P_L and P_M ($\Delta\alpha$) and the resonance integral β_D between P_L and P_M (see text). This value is obtained from Figure 8 using the measured spin density ratios ϱ_L/ϱ_M. [d] Difference of the orbital energies (Coulomb energies) of P_L and P_M (see text). [e] Shifts of $\Delta\alpha$ in the mutants with respect to the wild-type. [f] Midpoint potential E_m for the oxidation P/P^+. The free energy of the reaction cyt c_2^{2+} P^+ → cyt c_2^{3+} P is given by the difference of redox potentials E_m(cyt c_2^{2+}/cyt c_2^{3+}) − E_m(P/P^+) in eV (Lin et al., 1994a,b). [g] Electron trnasfer time for the reaction cyt $c_2^{2+}P^+$ → cyt $c_2^{3+}P$ (Lin et al., 1994).

The formation of this hydrogen bond has also been confirmed by FTIR (Nabedryk et al., 1993) and FT resonance Raman (Mattioli et al., 1994) experiments, in which a downshift of the vibrational frequency of the 9-keto group of P_M has been observed. Mattioli et al. (1994) also conclude that LH(M160) exhibits a more asymmetric charge distribution (~80%) in favor of P_L in $P^{\bullet+}$. This value is in excellent agreement with the one obtained by ENDOR (see Table 1).

For the almost symmetric spin density distribution in $P^{\bullet+}$ of LH(L131) the ratio ϱ_L/ϱ_M is 0.89. This results in a negative value for $\Delta\alpha/\beta_D$ = −0.05 showing that the HOMO of P_M is now by −67 meV below that of P_L, and $\Delta\alpha$ = −8 meV (see Figure 8). This effect can be explained by the formation of the hydrogen bond between the histidine introduced at position L131 and the 9-keto group of P_L. This energetically stabilizes this moiety and leads to almost equal energies of the HOMOs, i.e., to a fairly symmetric dimer. The formation of this hydrogen bond was independently confirmed by a downshift of the frequency of the vibration of the 9-keto group of P_L by FTIR (Nabedryk et al., 1993) and FT resonance Raman spectroscopy (Mattioli et al., 1994).

With a ratio ϱ_L/ϱ_M of 2.21 the spin density distribution in the double mutant LH(L131) + LH(M160) is comparable to that of the wild type. The value of $\Delta\alpha/\beta_D$ is 0.41 and $\Delta\alpha$ = 65 meV (see Table 6). This value differs only by + 6 meV from the wild type. Since the formation of both hydrogen bonds has been reported in the double mutant (Nabedryk et al., 1993; Mattioli et al., 1994), our results indicate an additive effect of the two mutations on the spin density distribution of $P^{\bullet+}$. Here, both dimer halves are lowered in energy by approximately the same amount (see Table 6) leading to a spin density distribution comparable

to that of the wild type. Thus, the effects of the two hydrogen bonds compensate each other with respect to the *spin density distribution* in $P^{\bullet+}$, which is only sensitive to the energetic difference $\Delta\alpha$, but not to the absolute value of the orbital energies, E_L or E_M. That the absolute value of the energies is changed can be seen from the change of the redox potential in the double mutant (Lin et al., 1994a), which is the sum of the changes found for the single-site mutations (see Table 6).

Mutations in the Vicinity of the 2-Acetyl Groups. In analogy to the mutants that form hydrogen bonds to the 9-keto oxygens of $P^{\bullet+}$, the intended cleavage of the hydrogen bond between His L168 and the 2-acetyl group of P_L is expected to raise the energy of the HOMO of P_L, leading to a more asymmetric spin density distribution in $P^{\bullet+}$ compared with the wild type. Instead, the spectrum of $P^{\bullet+}$ in HF(L168) (Figure 4) reveals a more symmetric dimer that even has a small excess of the spin density on P_M (57%), which implies that the energy of the HOMO of P_L is lowered by -79 meV and is below that of P_M (see Table 6).

The removal of the hydrogen bond between His L168 and the 2-acetyl group of P_L was supported by FT resonance Raman spectroscopy (Mattioli et al., 1994), where a shift of the carbonyl vibrational frequency of the 2-acetyl group of P_L was observed. Mattioli et al. (1994) also drew the conclusion that the charge distribution is more symmetric in $P^{\bullet+}$ of HF(L168) than in the wild type. Obviously, the picture describing the energetics of the dimer halves constituting the primary donor is more complicated for the mutations near the 2-acetyl groups. This is due to the fact that this group can rotate about the 2−2a bond. MO calculations (RHF INDO/SP) (Plato et al., 1986, 1992) showed that the orientation of the 2-acetyl group has a major effect on the energy difference $\Delta\alpha$ between the dimer halves P_L and P_M. It has been proposed that different dihedral angles θ_{ac} of the acetyl groups (see Figure 1) of P_L and P_M could be the main reason of the energetic difference of the respective MOs in the wild type (Plato et al., 1992; Lendzian et al., 1993). The formation of the hydrogen bond to His L168 forces the 2-acetyl group of P_L to rotate out of the molecular plane. On the basis of RHF-INDO/SP calculations with energy minimization, Plato et al. (1992) found a value of $\theta_{ac} = 45°$. That the 2-acetyl group of P_L is out of plane and hydrogen bonded to residue His L168 is also confirmed by the recent X-ray structure of Ermler et al. (1994a). The removal of this hydrogen bond allows the 2-acetyl group of P_L to rotate to a more in-plane position and to become part of the conjugated π-system, thereby lowering the energy of the HOMO of $P^{\bullet+}$. In the mutants intended to change the hydrogen bond situation to the acetyl groups, one has to account for two parameters influencing the energetics of the dimer. In the case of $P^{\bullet+}$ in HF(L168) we suggest that the lowering of the HOMO of P_L is caused by a more in-plane position of the acetyl group, which overcompensates the expected raise of E_L due to the lack of the hydrogen bond. As proposed earlier (Plato et al., 1986, 1992) a dimer with no hydrogen bonds, like HF(L168), is expected to exhibit an almost symmetric spin density distribution of $P^{\bullet+}$.

In a semiempirical calculation of the position of the Q_y-band of the primary donor in RCs of *Rps. viridis* as a function of the dihedral angle θ_{ac} Parson and Warshel (Parson & Warshel, 1987; Warshel & Parson, 1987) found that a rotation of the 2-acetyl group of P_L, which is in-plane in *Rps. viridis*, to a position out of plane leads to a red-shift of the Q_y-band of P. Assuming that the dependence of the Q_y-band of P on the dihedral angle θ_{ac} is similar in RCs of *Rb. sphaeroides*, the rotation of the 2-acetyl group of P_L to a more in-plane position should lead to a blue-shift of this band. The inspection of the optical absorption spectra of the various mutants provides further evidence for a reorientation of the 2-acetyl group toward a more in-plane position. The optical absorption spectra of HF(L168) and *all* double mutants that contain HF(L168) as one of the mutations show a blue-shift of the Q_y-band of P of 20−40 nm (Mattioli et al., 1995), whereas in all other single and double mutants the position of the Q_y-band of the primary donor is similar to that of the wild type.

From the comparison of the Special TRIPLE spectra of the mutant FH(M197) with the wild type, it is not obvious that the intended hydrogen bond between the introduced residue His M197 and the 2-acetyl group of P_M is formed. However, the redox potential for this mutant is drastically altered (see Table 6; Lin et al., 1994a). FT resonance Raman experiments on this mutant indeed show the formation of a strong hydrogen bond to this group (Mattioli et al., 1994). Such a hydrogen bond is expected to lower the energy of the HOMO of P_M, which should result in a dimer with more spin density on P_L. This is not observed in the Special TRIPLE spectrum of FH(M197). An explanation is provided by assuming a reorientation of the 2-acetyl group of P_M upon hydrogen bond formation. According to the RHF-INDO/SP calculations of Plato et al. (1992), the 2-acetyl group of P_M has an almost in plane position in the wild type with a dihedral angle of $\theta_{ac} = 6°$. After hydrogen bond formation, this group is expected to rotate out of the molecular plane, thereby increasing the energy of the HOMO of P_M. Obviously, this rotation compensates the expected decrease of the orbital energy due to the hydrogen bond formation. Another indication that this could indeed be the case is the altered ratio of the methyl couplings $A(5a)/A(1a)$ of P_M, which is 1.98 (Table 2). This value changes depending on the rotation angle of the 2-acetyl group in the BChl *a* cation (W. Lubitz, unpublished results). It is, however, puzzling that this rotation does not cause a red-shift of the Q_y absorption band of P, like in the HF(L168) mutants.

An alternate explanation of the observed effects in FH(M197) could be provided by a ligation of the 2-acetyl group of P_M to the central Mg^{2+} ion of P_L in the wild type, as was first proposed for *Rps. viridis* (Deisenhofer et al., 1984) and also discussed for *Rb. sphaeroides* (Robert & Lutz, 1986; Zhou et al., 1987). Such a ligation is also discussed in the recently published X-ray structure of *Rb. sphaeroides* by Ermler et al. (1994a). A ligation to the central Mg^{2+} of P_L would rotate this group of P_M out of the molecular plane. Formation of the hydrogen bond to His M197 could rotate the acetly group in the opposite direction but with an out of plane angle similar to the value in the wild type. If the hydrogen bond strength is comparable to the energy of the ligation to Mg^{2+}, only a small change in the spin density distribution would be expected. As in the case of LH(L131) + LH(M160), the effects observed for the double mutant HF(L168) + FH(M197) can be interpreted as arising from the superposition of the effects of the respective single mutations.

Since the 2-acetyl groups are in the overlap region of the two BChl macrocycles constituting the dimer, an influence

of the rotation of these groups on the value of the resonance integral β_D could be expected. However, the β_D values calculated from the experimental spin density ratios and the ΔE values (E. Nabedryk, unpublished results) indicate that this is not the case.

Combined Double Mutations. Williams et al. (1992b) showed that the formation or removal of a hydrogen bond donor alters the P/P^+ oxidation midpoint potential for the single mutations. In the double mutants the values of the oxidation midpoint potentials are additive with regard to the single mutants (Lin et al., 1994a) and correlate with the total change in hydrogen bonding energy (Mattioli et al., 1995). This shows that the intended hydrogen bonds are also formed or cleaved in the double mutants.

In the case of LH(M160) + FH(M197), the P/P^+ oxidation midpoint potential of 700 mV (Lin et al., 1994a) indicates that the primary donor in this mutant posseses a total of three hydrogen bonds. The asymmetric spin density distribution in favor of P_L with $\varrho_L/\varrho_M = 4.87$ yields a $\Delta\alpha$ of 142 meV. This is very close to the respective value of the single mutant LH(M160) (see Table 6). As was shown for the single mutant FH(M197), the effects of the hydrogen bond between His M197 and the 2-acetyl group of P_M on the spin density distribution compensate each other and result in a Special TRIPLE spectrum of $P^{\bullet+}$ which is similar to the wild type. Therefore the spin density distribution of $P^{\bullet+}$ in the double mutant LH(M160) + FH(M197) can be fully understood as the superposition of the effects of the single mutations.

The P/P^+ oxidation midpoint potential of 485 mV for the double mutant LH(M160) + HF(L168), which is close to that of the wild type (505 mV), points toward the presence of only one hydrogen bond (Lin, 1994a). The evalution of the spin density distribution given in Table 6 reveals only small deviation from the values for the wild type. This spin density distribution can be understood by an inspection of the effects of the single mutation LH(M160), which results in a strongly asymmetric dimer (see Table 6) in combination with the single mutation HF(L168) that has a nearly symmetric dimer. The combination of these two mutants leads to compensating effects on the energetics of the dimer, resulting in an only slightly more asymmetric spin distribution than in the wild type.

The high P/P^+ oxidation midpoint potential of 710 mV measured for the double mutant LH(L131) + FH(M197) (Lin et al., 1994a) is very similar to that of LH(M160) + FH(M197). This is good evidence for the formation of the intended two new hydrogen bonds to the primary donor. With the assignment of the methyl couplings given in Table 3, the ratio of $\varrho_L/\varrho_M = 0.68$ results in a ratio of $\Delta\alpha/\beta_D = -0.18$, which shows that an excess of spin density is on P_M caused by a decrease of the energy of the HOMO of P_L below that of P_M. The formation of the hydrogen bond between the histidine at position L131 and the 9-keto carbonyl of P_L lowers the HOMO of P_L by 88 meV compared to the wild type. The second mutation FH(M197) does not significantly alter the spin density distribution of $P^{\bullet+}$ as in the other mutants (see above).

A very nice example for the additivity of the effects of the single mutations is provided by the double mutant LH(L131) + HF(L168). The Special TRIPLE spectrum of this species shows an excess of the unpaired electron on P_M. Since both single mutations cause a decrease of the energy of the HOMO of P_L, the combination of the two mutations lowers the HOMO of P_L by −167 meV (see Table 6). This results in a spin density distribution of 78% on P_M.

Influence of Hydrogen Bonds on the Heterodimer. The spectra of the mutants that combine the heterodimer mutant with the two mutations LH(L131) and HF(L168) can be understood by the effects of the formation or removal of a hydrogen bond to the L-half BChl moiety of $P^{\bullet+}$.

In the case of HL(M202) + LH(L131) the RHF-INDO/SP calculations on the BChl *a* cation radical (W. Lubitz, unpublished results) showed that the formation of a hydrogen bond to the 9-keto group causes an upshift in the hfc of the neighboring methyl protons 5a while the opposite methyl hfc of 1a remains unchanged. The increase of A(5a) by approximately 10% and the unchanged value of A(1a) for P_L in HL(M202) + LH(L131) therefore indicate that in $P^{\bullet+}$ a hydogen bond between His L131 and the oxygen of the keto group in P_L is formed.

In the case of HL(M202) + HF(L168) the cleavage of the hydrogen bond between the residue His L168 and the 2-acetyl group of P_L causes a decrease of the hfcs A(1a) of the neighboring methyl protons by ~5% while the opposite methyl hfc A(5a) remains unchanged in agreement with RHF-INDO/SP calculations.

The spectra of the double mutants HL(M202) + LH(M160) and HL(M202) + FH(M197) with hydrogen bonds to the BPhe P_M are identical within experimental errors to that of the heterodimer HL(M202).

These results indicate that the energetic changes introduced through the hydrogen bonds do not lead to a shift of spin density between the two dimer halves of the heterodimer. Clearly, the simple picture of the dimer model is no longer valid here, since the energetic difference of the HOMOs of the BChl and the BPhe in the heterodimer is too large. This view is also confirmed by the absence of the new band for HL(M202) and for all four double mutants (Nabedryk et al., 1995).

Relation between Orbital Asymmetry in $P^{\bullet+}$ and ET Rates in the RC. An interesting question is whether the ET rates in the RC are influenced by the different orbital asymmetries of $P^{\bullet+}$ in the various mutants. These rates are proportional to the square of the matrix element of the electronic coupling between donor and acceptor molecule and to the Franck−Condon factor, which depends exponentially on $\Delta G°$, the free energy, and λ, the reorganization energy of the reaction (Marcus & Sutin, 1985). If the electronic coupling between $P^{\bullet+}$ and the ET partner molecule occurs mainly via one dimer half, P_L or P_M, the ET rate should also depend on the fraction of spin (hole) density on this dimer half. A similar effect on the rate is expected, if the reorganization energy λ is different for a localization of the spin (and charge) on P_L or P_M. Effects on the rates are expected mainly for secondary ET reactions which lead to a reduction of $P^{\bullet+}$. These are, for example, the charge recombination $P^{\bullet+}Q_A^{\bullet-} \rightarrow PQ_A$ and the reduction by cytochrome cyt c_2^{2+} $P^{\bullet+} \rightarrow$ cyt c_2^{3+} P. The rates for the latter reaction have recently been measured for all mutants studied in this paper by Lin et al. (1994b). The observed rates change by two orders of magnitude in the series of these mutants (Table 6). They are mainly determined by the different $\Delta G°$ values, which are in good approximation given by the difference of the redox potential of cyt c_2^{2+}/cyt c_2^{3+} (345 mV) and the redox potential of $P/P^{\bullet+}$ for the respective mutants (see Table 6). However, compar-

ing the experimental ET rates with the fit to the Marcus equation (Lin et al., 1994b), one finds that in all cases with excess spin (hole) density on P_M the rates are significantly smaller than theoretically expected. This is particularly pronounced for the mutants HF(L168) + LH(L131) (78% localized on P_M) and LH(M160) + HF(L168) (70% localized on P_L), which have the same $\Delta G°$ value but differ by more than a factor of 3 in the rates (Table 6). Interestingly, the fraction of spin density on P_L differs by exactly the same factor (Table 6). A similar behavior is observed for several other mutants. Therefore, in addition to the expected exponential dependence on $\Delta G°$, the ET rates are found to be approximately proportional to the fraction of spin density on P_L. Structural data obtained from co-crystals of the RC of *Rb. sphaeroides* and cyt c_2 show that the latter is in close contact with the M subunit (Adir et al., 1994). Our data indicate that electron transfer from the heme proceeds preferentially to the L half of the dimer. This could be due to a smaller edge-to-edge distance of these cofactors or specific electronic interactions involving the protein which facilitate this pathway. This is currently being investigated in more detail in our laboratories.

CONCLUSIONS

The influence of hydrogen bonds on the spin density distribution of the primary donor cation radical $P^{\bullet+}$ has been investigated by ENDOR and TRIPLE resonance for a series of mutants exhibiting different combinations of hydrogen bonds to the four carbonyl oxygens of the BChl dimer. In the case of mutants, where the spin density is fully localized on one half of the dimer [e.g., in the heterodimer mutant HL(M202)], only small redistributions of spin densities were observed within the spin-carrying BChl *a* moiety. Here, the hydrogen bonds to the carbonyl groups of ring I or V lead to an increase of the adjacent methyl proton hfcs (positions 1a and 5a; see Figure 1) by $\leq 10\%$.

In the case of the other mutants, in which P consists of two BChl *a* molecules, large shifts of spin density *between* the two dimer halves P_L and P_M were observed, ranging from 83% on P_L to 78% on P_M. This finding was interpreted by an asymmetric dimer model with different energies for the HOMOs of P_L and P_M caused by different hydrogen bond situations. The asymmetry of the spin density distribution in the supermolecular orbital depends on the ratio $\Delta\alpha/\beta_D$, where $\Delta\alpha$ is the difference of the Coulomb energies of P_L and P_M, and β_D is the resonance integral between the two halves (Plato et al., 1992; Lendzian et al., 1993). Using a constant β_D of 160 meV for all investigated mutants, an average shift, $\delta(\Delta\alpha) \approx -80$ meV was found for the formation of each hydrogen bond to the keto group in position 9 (Table 6). For the acetyl group oxygens, additional energetic contributions result from an out-of-plane rotation of this substituent induced by the hydrogen bond.

The distribution of the spin densities in $P^{\bullet+}$ also reflects the distribution of the hole, i.e., the positive charge in the supermolecule. Thus, ET reactions leading to the reduction of $P^{\bullet+}$ may be affected by the different spin density ratios. We found that the published electron transfer rates from cyt c_2^{2+} to P^+ in these mutants (Lin et al., 1994b) show deviations from the exponential dependence on $\Delta G°$ which correlate with the fraction of the electron spin on P_L. This provides interesting aspects for theoretical calculations of the electron pathway between the heme in cyt c_2 and the primary donor in *Rb. sphaeroides*.

ACKNOWLEDGMENT

We are grateful to I. Geisenheimer and U. Fink (both Technische Universität Berlin) for their help with the mutagenesis, cultivation of bacteria, and reaction center isolation. We thank Drs. E. Nabedryk and J. Breton (CEA, Saclay) for communicating IR data prior to publication. Many helpful discussions with M. Plato (Freie Universität Berlin) concerning the dimer model are gratefully acknowledged.

REFERENCES

Adir, N., Okamura, M. Y., & Feher, G. (1994) *Biophys. J. 66*, A127.
Allen, J. P., Feher, G., Yeates, T. O., Komiya, H., & Rees, D. C. (1987) *Proc. Natl. Acad. Sci. U.S.A. 84*, 5730−5734.
Allendoerfer, R. D., & Maki, A. G. (1970) *J. Magn. Reson. 3*, 396−410.
Breton, J., Nabedryk, E., & Parson, W. W. (1992) *Biochemistry 31*, 7503−7510.
Bylina, E. J., & Youvan, D. C. (1988) *Proc. Natl. Acad. Sci. U.S.A. 85*, 7226−7230.
Chirino, A. J., Lous, E. J., Huber, M., Allen, J. P., Schenck, C. C., Paddock, M. L., Feher, G., & Rees, D. C. (1994) *Biochemistry 33*, 4584−4593.
Deisenhofer, J., Epp, O., Miki, K., Huber, R., & Michel, H. (1984) *J. Mol. Biol. 180*, 385−398.
El-Kabbani, O., Chang, C. H., Tiede, D., Norris, J., & Schiffer, M. (1991) *Biochemistry 30*, 5361−5369.
Ermler, U., Fritzsch, G., Buchanan, S., & Michel, H. (1992) in *Research in Photosynthesis* (Murata, N., Ed.) Vol. 1, pp 341−347, Kluwer Academic Press, The Netherlands.
Ermler, U., Fritzsch, G., Buchanan, S. K., & Michel, H. (1994a) *Structure 2*, 925−936.
Ermler, U., Michel, H., & Schiffer, M. (1994b) *J. Bioenenerg. Biomembr. 26*, 5−15.
Fajer, J., Brune, D. C., Davies, M. S., Forman, A., & Spaulding, L. D. (1975) *Proc. Natl. Acad. Sci. U.S.A. 72*, 4956−4960.
Feher, G. (1992) *J. Chem. Soc., Perkin Trans. 2 11*, 1861−1874.
Feher, G., & Okamura, M. Y. (1978) in *The Photosynthetic Bacteria* (Clayton, R. K., & Sistrom, W. R., Eds.) pp 349−386, Plenum Press, New York.
Feher, G., Hoff, A. J., Isaacson, R. A., & Ackerson, L. A. (1975) *Ann. N.Y. Acad. Sci. 244*, 239−259.
Feher, G., Allen, J. P., Okamura, M. Y., & Rees, D. C. (1989) *Nature 339*, 111−116.
Gessner, C., Lendzian, F., Bönigk, B., Plato, M., Möblus, K., & Lubitz, W. (1992) *Appl. Magn. Reson. 3*, 763−777.
Hoff, A. (1993) in *The Photosynthetic Reaction Center* (Deisenhofer, J., & Norris, J. R., Eds.) Vol. II, pp 331−386, Academic Press, New York.
Huber, M., Lous, E. J., Isaacson, R. A., Feher, G., Gaul, D., & Schenck, C. C. (1990) in *Reaction Centers of Photosynthetic Bacteria* (Michel-Beyerle, M. E., Ed.) pp 219−228, Springer, Berlin.
Hyde, J. S., Rist, G. H., & Eriksson, L. E. G. (1968) *J. Phys. Chem. 72*, 4269.
Käss, H., Rautter, J., Zweygart, W., Struck, A., Scheer, H., & Lubitz, W. (1994) *J. Phys. Chem. 98*, 354−363.
Käss, H., Rautter, J., Bönigk, B., Höfer, P., & Lubitz, W. (1995) *J. Phys. Chem. 99*, 436−448.
Kunkel, T. A., Roberts, J. D., & Zakour, R. A. (1987) *Methods Enzymol. 154*, 367−382.
Lendzian, F., Lubitz, W., Scheer, H., Hoff, A. J., Plato, M., Tränkle, E., & Möbius, K. (1988) *Chem. Phys. Lett. 148*, 377−385.
Lendzian, F., Huber, M., Isaacson, R. A., Endeward, B., Bönigk, B., Möbius, K., Lubitz, W., & Feher, G. (1993) *Biochim. Biophys. Acta 1183*, 139−160.
Lin, X., Murchison, H. A., Nagarajan, V., Parson, W. W., Williams, J. C., & Allen, J. P. (1994a) *Proc. Natl. Acad. Sci. U.S.A. 91*, 10265−10269.

Lin, X., Williams, J. C., Allen, J. P., & Mathis, P. (1994b) *Biochemistry 33*, 13517−13523.
Lubitz, W. (1991) in *Chlorophylls* (Scheer, H., Ed.) pp 903−944, CRC Press, Boca Raton, FL.
Mattioli, T. A., Williams, J. C., Allen, J. P., & Robert, B. (1994) *Biochemistry 33*, 1636−1643.
Mattioli, T. A., Lin, X., Allen, J. P., & Williams, J. C. (1995) *Biochemistry 34*, 6142−6152.
Möbius, K., Lubitz, W. & Plato, M. (1989) in *Advanced EPR* (Hoff, A. J., Ed.) pp 441−499, Elsevier, Amsterdam.
Murchison, H. A., Alden, R. G., Allen, J. P., Peloquin, J. M., Taguchi, A. K. W., Woodbury, N. W., & Williams, J. C. (1993) *Biochemistry 32*, 3498−3505.
Nabedryk, E., Allen, J. P., Taguchi, A. K. W., Williams, J. C., Woodbury, N. W., & Breton, J. (1993) *Biochemistry 32*, 13879−13885.
Nabedryk, E., Breton, J., Kuhn, M., Fetsch, A., Schulz, C., & Lubitz, W. (1995) *Biophys. J. 68*, A93.
Paddock, M. L., Rongey, S. H., Feher, G., & Okamura, M. Y. (1989) *Proc. Natl. Acad. Sci. U.S.A. 86*, 6602−6606.
Parson, W. W., & Warshel, A. (1987) *J. Am. Chem. Soc. 109*, 6152−6163.
Plato, M., Tränkle, E., Lubitz, W., Lendzian, F., & Möbius, K. (1986) *Chem. Phys. 107*, 185−196.
Plato, M., Lendzian, F., Lubitz, W., & Möbius, K. (1992) in *The Photosynthetic Bacterial Reaction Center II: Structure, Spectroscopy and Dynamics* (Breton, J., & Vermeglio, A., Eds.) pp 109−118, Plenum Press, New York.
Rautter, J., Gessner, C., Lendzian, F., Lubitz, W., Williams, J. C., Murchison, H.A., Wang, S., Woodbury, N. W., & Allen, J. C. (1992) in *The Photosynthetic Bacterial Reaction Center* II: *Structure, Spectroscopy and Dynamics* (Breton, J., & Vermeglio, A., Eds.) pp 99−108, Plenum Press, New York.
Rautter, J., Lendzian, F., Wang, S., Allen, J. P., & Lubitz, W. (1994) *Biochemistry 33*, 12077−12084.
Robert, B., & Lutz, M. (1986) *Biochemistry 25*, 2303−2309.
Sambrook, J., Fritsch, E. F., & Maniatis, T. (1989) *Molecular Cloning: A Laboratory Manual*, Cold Spring Harbor Laboratory Press, Cold Spring Harbor, NY.
Sanger, F., Nicklen, S., & Coulsen, A. R. (1977) *Proc. Natl. Acad. Sci. U.S.A. 80*, 6505−6509.
Schenck, C. C., Gaul, D., Steffen, M., Boxer, S. G., McDowell, L., Kirmaler, C., & Holten, D. (1990) in *Reaction Centers of Photosynthetic Bacteria* (Michel-Beyerle, M. E., Ed.) pp 229−238, Springer, Berlin.
Stocker, J. W., Taguchi, A. K. W., Murchison, H. A., Woodbury, N. W., & Boxer, S. G. (1992) *Biochemistry 31*, 10356−10362.
Tränkle, E., & Lendzian, F. (1989) *J. Magn. Reson. 84*, 537−547.
Vandeyar, M. A., Weiner, M. P., Hutton, C. J., & Batt, C. A. (1988) *Gene 65*, 129−133.
Warshel, A., & Parson, W. W. (1987) *J. Am. Chem. Soc. 109*, 6143−6152.
Williams, J. C., Alden, R. G., Coryell, V. H., Lin, X., Murchlson, H. A., Peloquin, J. M., Woodbury, N. W., & Allen, J. P. (1992a) in *Research in Photosynthesis* (Murata, N., Ed.) Vol. 1, pp 377−380, Kluwer Academic Press, Dordrecht, The Netherlands.
Williams, J. C., Alden, R. G., Murchison, H. A., Peloquin, J. M., Woodbury, N. W., & Allen, J. P. (1992b) *Biochemistry 31*, 11029−11037.
Zhou, Q., Robert, B., & Lutz, M. (1987) *Biochim. Biophys. Acta 890*, 368−376.
Zweygart, W., Thanner, R., & Lubitz, W. (1994) *J. Magn. Reson. A109*, 172−176.

BI9504670